ACCOUNTS
of chemical research

Nanoparticle ζ -Potentials

TENNYSON L. DOANE,[†] CHI-HUNG CHUANG,[†] REGHAN J. HILL,[*,‡] AND CLEMENS BURDA[*,†]

[†]*Department of Chemistry, Case Western Reserve University, 10900 Euclid Avenue, Cleveland, Ohio 44106, United States, and* [‡]*Department of Chemical Engineering, McGill University, 3610 University Street, Montreal, QC, Canada H3A 2B2*

RECEIVED ON APRIL 13, 2011

CONSPECTUS

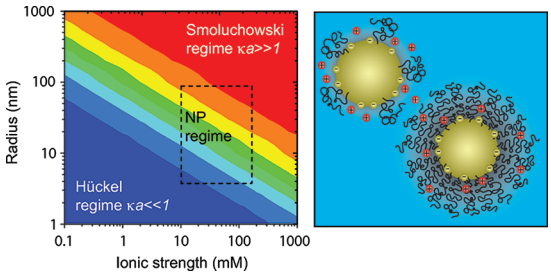

For over half a century, alternating electric fields have been used to induce particle transport, furnishing the ζ-potential of analytes with sizes ranging from a few nanometers to several micrometers. Concurrent advances in nanotechnology have provided new materials for catalysis, self-assembly, and biomedical applications, all of which benefit from a thorough understanding of particle surface charge.

Therefore, the measurement of the ζ-potential via electrophoretic light scattering (ELS) has become essential for nanoparticle (NP) research. However, the interpretation of NP electrophoretic mobility, especially that of ligand-coated NPs, can be a complex undertaking. Despite the inherent intricacy of these data, key concepts from colloidal science can help to distill valuable information from ELS.

In this Account, we adopt PEGylated Au NPs as an illustrative example to explore extensions of the classical theories of Smoluchowski, Hückel, and Henry to more contemporary theories for ligand-coated NP systems such as those from Ohshima, and Hill, Saville, and Russel. First, we review the basic experimental considerations necessary to understand NP electrophoretic mobility, identifying when O'Brien and White's numerical solution of the standard electrokinetic model should be adopted over Henry's closed-form analytical approximation. Next, we explore recent developments in the theory of ligand-coated particle electrophoresis, and how one can furnish accurate and meaningful relationships between measured NP mobility, ζ-potential, and surface charge. By identifying key ligand-coated NP parameters (e.g., coating thickness, permeability, molecular mass, and hydrodynamic segment size), we present a systematic method for quantitatively interpreting NP electrophoretic mobility.

In addition to reviewing theoretical foundations, we describe our recent results that examine how the unique surface curvature of NPs alters and controls their properties. These data provide guidelines that can expedite the rational design of NPs for advanced uses, such as heterogeneous catalysis and in vivo drug delivery. As a practical demonstration of these concepts, we apply the ligand-coated theory to a recently developed noncovalent PEGylated Au NP drug-delivery system. Our analysis suggests that anion adsorption on the Au NP core may enhance the stability of these NP—drug conjugates in solution.

In addition to providing useful nanochemistry insights, the information in this Account will be useful to biomedical and materials engineers, who use ELS and ζ-potentials for understanding NP dynamics.

1. Electrophoretic Light Scattering

Nanoparticle (NP) surface charge is of fundamental importance to many research areas, including electrophoretic deposition,[1] self-assembly,[2] and biological[3] applications. In solution, the surface charge (which can be inherent to the NP or the result of ion adsorption)[4] is shielded by a diffuse layer of solvated counterions. The electrostatic surface potential, termed the ζ-potential (ζ), is highly dependent on the immediate environment. Together, the fixed surface charge and diffuse layers are termed the "double layer".

"Smooth" interfaces exhibiting a disparity between the electrokinetic and actual surface charge (e.g., as ascertained

Published on the Web 11/10/2011 www.pubs.acs.org/accounts
10.1021/ar200113c

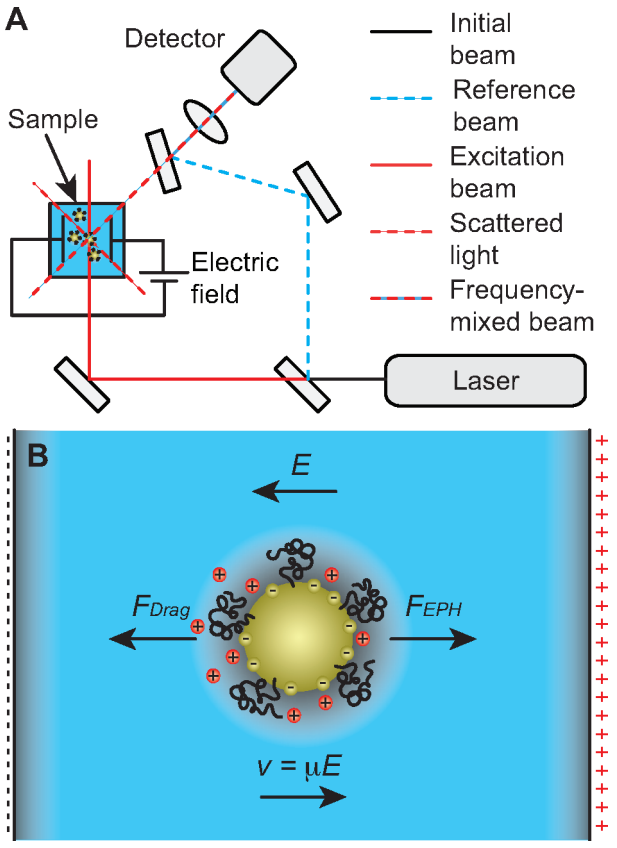

FIGURE 1. (A) Schematic (heterodyne) electrophoretic light scattering (ELS) setup.[10] (B) Negatively charged particle migrating with velocity $\vec{v}$ when subjected to an electric field $\vec{E}$ between an anode (right) and cathode: $\vec{F}_{EPH}$ is the electrophoretic force, and $\vec{F}_{Drag}$ is the solvent drag force. Particles migrate at constant velocity while experiencing zero net force.[13]

by titration) may be subject to anomalous surface conduction or Stern-layer conduction.[5] Here, charge within the Stern layer (i.e., behind the slipping plane) is mobile, allowing the surface charge and, hence, the electrical force to dynamically respond to an applied electric field. While such models improve correspondence between theory and experiments, ascertaining the Stern-layer model parameters (e.g., ion mobilities and capacitances) is demanding.

NP ζ-potentials are routinely obtained from electrophoretic light scattering (ELS), but interpreting the ζ-potential of particles with sizes in the range 5−100 nm presents a delicate challenge.[6] Ligand-coated NPs provide further complexity, because the hydrodynamic size and surface-charge shielding depend on the ligand conformation.

We begin by describing the theory underlying the most common conversion of ELS mobility data to ζ-potential, building off the well-known, but not always appropriately used, Smoluchowski formula.[7] We present two important extremes of bare and uncharged polymer-capped NPs, accounting for electrolyte ionic strength, polymer-layer thickness, and surface curvature. Gold nanoparticles (Au NPs) with a neutral ligand polyethylene glycol (PEG) are adopted as an example, but the discussion applies to other nanometer size analytes relevant to macromolecular[8] and biomedical research.[9]

In an ELS experiment, a laser beam is split into reference and excitation beams. The excitation beam is directed through the sample (Figure 1A) while an electric field $\vec{E}$ is applied to induce NP electrophoresis (Figure 1B).[10] Upon recombination of the scattered and reference beams, a difference frequency is produced, which is measured by the ELS detector to provide the particle electrophoretic drift velocity $\vec{v}$.[10,11] Even though an alternating electric field (at kHz frequencies) is often applied, the NP response at sub-MHz frequencies is quasi-steady.[12]

Au NPs furnish a valuable ELS example, because they are an important analyte for the application of ELS to contemporary research. Daniel and Astruc recently reviewed the history and physical properties of Au NPs, including practical synthesis procedures.[14] Au NPs are advantageous because of their low toxicity and chemical inertness, allowing for ligand-exchange reactions that provide further control parameters.[3] In addition, ζ-potential measurements of "bare"[15] and polymer-capped Au NPs have been reported.[16−18] As a typical application of ζ-potential measurements and the ELS technique, we address how understanding the surface charge could improve the emerging field of PEGylated Au NP based drug delivery.

2. Electrophoresis of Bare Nanoparticles

The particle electrophoretic velocity (Figure 1) is customarily written[19]

$$\vec{v} = \mu\vec{E} \qquad (1)$$

where μ (a scalar for isotropic particles, but more generally a second-order tensor) is termed the *electrophoretic mobility*. In turn, the mobility is often expressed in terms of a ζ-potential (reported in mV) via Smoluchowski's famous formula[7]

$$\mu = \varepsilon\varepsilon_0\eta^{-1}\zeta \quad (\kappa a \gg 1) \qquad (2)$$

where ε is the solvent dielectric constant (≈80 for water at 25 °C), $\varepsilon_0 \approx 8.854 \times 10^{-12}$ C^2 N^{-1} m^{-2} is the vacuum permittivity, and η is the solvent viscosity (≈8.9×10^{-4} Pa s for water at 25 °C). However, when converting the measured mobility to a ζ-potential, considerable care must be taken to obtain an accurate representation of the surface charge.[11] Moreover, the term "ζ-potential" is not always synonymous with the concept of "surface

charge", because the former describes the potential at the so-called "slipping plane" while the latter is the surface-localized charge behind the slipping plane.[6] More generally, ζ-potential is better considered a measure of "electrokinetic charge".

We begin by considering a "bare" spherical Au NP with radius a. The extent to which the immobile surface charge is screened by the electrolyte is determined by several parameters, most notably the solution ionic strength. For aqueous electrolytes at 25 °C, the Debye parameter κ (whose reciprocal κ^{-1} is termed the Debye screening length) for a symmetric electrolyte with ionic strength I is[20]

$$\kappa\ (\mathrm{nm}^{-1}) \approx 3.3[I(M)]^{1/2} \tag{3}$$

While Smoluchowski's formula furnishes the ζ-potential of micrometer-sized particles especially well, it is inappropriate when $\kappa a \ll 1$. Accordingly, Hückel[21] established

$$\mu = \frac{2}{3}\varepsilon\varepsilon_0\eta^{-1}\zeta \quad (|\zeta| < k_B T/e,\ \kappa a \ll 1) \tag{4}$$

where $k_B T$ is the thermal energy ($\approx 4.11 \times 10^{-21}$ J at 298 K) and $e \approx 1.602 \times 10^{-19}$ C is the fundamental charge. Here, viscous stresses arising form counterion migration (electroosmosis) opposite to the particle motion are negligible because of the vanishing counterion charge density when $\kappa a \ll 1$. Perhaps surprisingly, then, smaller particles migrate slower than larger ones with the same ζ-potential. Note, however, that the surface charge density is related to the ζ-potential by[19]

$$\sigma = \frac{\varepsilon\varepsilon_0 k_B T\zeta}{zea}(1 + \kappa a) \quad (|\zeta| < k_B T/e) \tag{5}$$

where z is the electrolyte valence (for z–z electrolytes). Thus, while smaller particles have a higher surface charge density, they still bear a lower charge $4\pi a^2\sigma \sim \zeta a(1 + \kappa a)$ under these conditions.

Henry[22] unified the foregoing Smoluchowski and Hückel regimes, showing that

$$\mu = \frac{2}{3}\varepsilon\varepsilon_0\eta^{-1}\zeta f_H(\kappa a) \tag{6}$$

where[19]

$$f_H(\kappa a) = \left\{1 + \frac{1}{16}(\kappa a)^2 - \frac{5}{48}(\kappa a)^3 - \frac{1}{96}(\kappa a)^4 + \frac{1}{96}(\kappa a)^5 + \left[\frac{1}{8}(\kappa a)^4 - \frac{1}{96}(\kappa a)^6\right]e^{\kappa a}E_1(\kappa a)\right\} \quad (|\zeta| < k_B T/e) \tag{7}$$

with $E_1(\kappa a)$ being an exponential integral. The Henry function $1 \le f_H(\kappa a) \le 3/2$ monotonically bridges the Hückel and Smoluchowski limits for any value of κa. Note, however, that the underlying Debye–Hückel linearization requires the magnitude of the ζ-potential to be less than the thermal voltage $k_B T/e \approx 25$ mV (at 25 °C). Moreover, the diffuse charge density is assumed to be unperturbed by the particle motion. By solving the standard electrokinetic model, numerically, O'Brien and White succeeded in removing these assumptions, showing that a qualitatively different behavior prevails when particles are highly charged.[25]

Ohshima derived a convenient approximation to Henry's formula[26]

$$f_H(\kappa a) = 1 + \frac{1}{2(1+\delta)^3} \tag{8}$$

with $\delta = 5/\{2\kappa a[1 + 2\exp(-\kappa a)]\}$. Ohshima also provides corrections for high ζ-potentials when $\kappa a < 10$ by accounting for diffuse-layer polarization, and O'Brien[28] provides asymptotic approximations for the mobility when $\kappa a \gg 1$, accounting for diffuse-layer polarization and multicomponent electrolytes. While ELS is restricted to dilute samples, electroacoustic instruments are available to measure electrophoretic mobilities (and particle size) in highly concentrated (turbid) dispersions.[12]

Henry's formula furnishes the most widely adopted relationship between bare NP mobilities and ζ-potential, accounting for the NP size and solution ionic strength. A contour plot of eq 8 is shown in Figure 2 identifying the Smoluchowski and Hückel regimes. The inset identifies an intermediate range ($a \sim 5$–100 nm and $I \sim 10$–150 mM) where NPs are commonly applied in technological and biomedical applications.[3,29] These regions are depicted in Figure 2B as an expansion (compression) of the Debye layer thickness upon decreasing (increasing) the ionic strength.

We have assumed that (i) the NP ζ-potential is independent of ionic strength and particle size (which has been demonstrated experimentally for bare Au NPs[30]) and (ii) the other experimental parameters (i.e., temperature, viscosity, solvent dielectric constant, and nonideal electrolyte behavior) are known constants. Even with these assumptions, correctly interpreting ELS data is challenging.

For example, whereas Henry's theory furnishes a monotonically varying mobility with respect to changes in ζ-potential and κa, numerical solutions of the standard

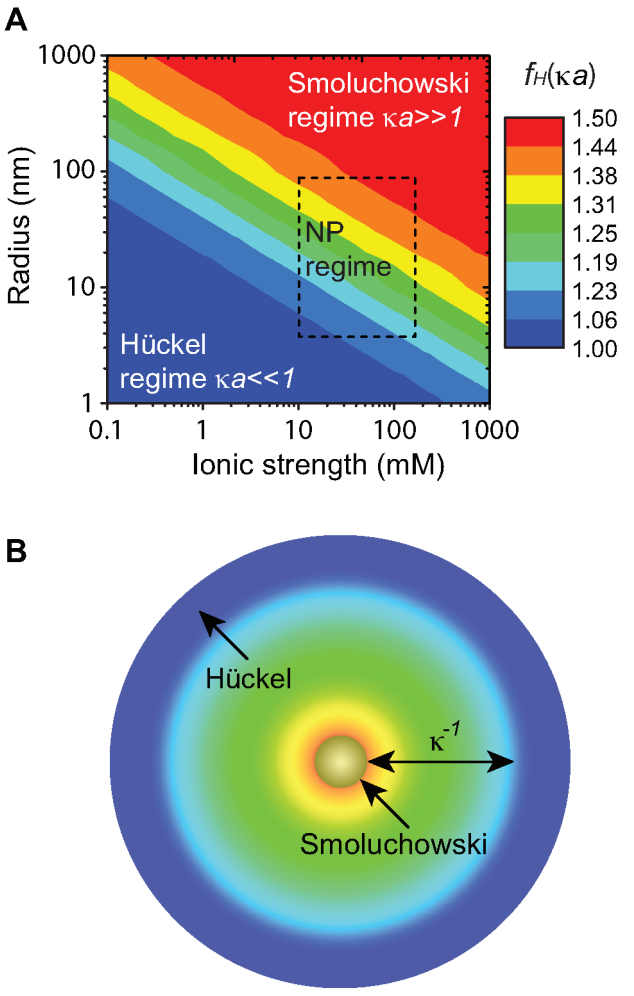

FIGURE 2. (A) Henry's factor $f_H(\kappa a)$ colored according to the analyte radius and solution ionic strength (both with logarithmic scales): the Smoluchowski $[f_H(\kappa a) = 3/2]$ and Hückel $[f_H(\kappa a) = 1]$ limits are identified by red and blue, respectively, with the rectangle identifying particle radii and ionic strengths prevailing in common NP applications. (B) The Debye layer thickness κ^{-1} colored according to the accompanying Henry factor $f_H(\kappa a)$ in (A).

electrokinetic model by O'Brien and White show that particles with different ζ-potentials can have the same mobility.[25] Interestingly, Khair and Squires recently demonstrated theoretically (for $\kappa a \gg 1$) that this "mobility maximum" vanishes at high ionic strengths if the model is extended to account for finite electrolyte ion size.[31] While similar conclusions might be drawn for soft particles, no calculations have yet been undertaken; nor is it known whether such inferences extend to particles with thicker diffuse layers ($\kappa a \lesssim 50$). Nevertheless, for NPs with $|\zeta| \lesssim 50$ mV, errors incurred by applying Henry's formula (adopting the Debye–Hückel linearization and neglecting diffuse-layer polarization) are generally comparable to instrumental precision. For highly charged particles, however, mobilities

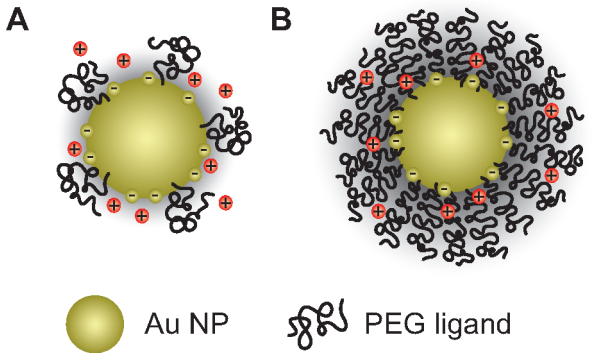

FIGURE 3. PEG chains grafted to a Au NP core adopt a "mushroom" configuration when the grafting density Γ_{PEG} is low (A) and extend into a "brush" when Γ_{PEG} is high (B).[37]

should be interpreted much more carefully to furnish meaningful ζ-potentials and, thus, surface charge densities.

We have also assumed that samples are monodisperse and, thus, free of aggregates. Since light scattering increases with particle size,[32] the mobility can be biased by the largest particles in a polydisperse sample. Efforts to synthesize monodisperse NP systems, and the complexities that come from polydispersity (e.g., temporal changes in surface charge and mass heterogeneity), are beyond the scope of this Account, but are active fields of research for NP transport in environmental and biomedical systems.

3. Polymer-Capped Nanoparticles

Many nanomaterials are not "bare", as addressed by the standard electrokinetic model, but are coated with a ligand corona. The changes in particle size and other physicochemical properties that accompany ligand attachment considerably complicate the interpretation of ELS mobility in terms of a ζ-potential. For this reason, ELS data are often used to identify qualitative changes in particle characteristics.[33,34] However, understanding the hydrodynamics, electrostatics, and polymer-conformation surrounding a particle is essential for achieving optimal control of these materials in applications.

To address concerns that arise during an ELS measurement involving ligand-capped NPs, we adopt commonly studied PEGylated Au NPs as an example. For these coatings, electrolyte pervades the polymer corona,[35] which hydrodynamically and sterically shields the Au NP core, increasing colloidal stability when repulsive electrostatic forces are weak compared to attractive van der Waals forces. The influences of PEG conformation and shielding depend on the grafting density Γ, ligand molecular weight *M*, and solvent. Figure 3 illustrates the qualitative influence of Γ on PEG

conformation in aqueous electrolytes. If Γ is sufficiently low (panel A), PEG chains adopt "mushroom" configurations,[36] whereas at high grafting densities (panel B) ligands minimize their collective free energy by extending into a "brush".[36,37]

When correlating the electrophoretic mobility μ to the ζ-potential, one needs to consider how the ligands increase hydrodynamic drag.[38−40] They clearly increase the NP hydrodynamic size (the composite sphere has a larger hydrodynamic size than the Au NP core) and, thus, increase the hydrodynamic drag force $\vec{F}_{\text{Drag}}$ (Figure 1). However, ligands also decrease the electrophoretic force $\vec{F}_{\text{EPH}}$ (Figure 1), because they hydrodynamically couple to the electroosmotic flow, producing a Darcy drag force[41] that increases the so-called *electrophoretic retardation* force. These effects depend on the ligand thickness L, the diffuse layer thickness κ^{-1}, and the ligand hydrodynamic permeability, as quantified by the Brinkman screening length ℓ_B.[41] In general, the increase in NP hydrodynamic size dominates when $\kappa L > 1$, and the Darcy drag dominates when $\kappa L < 1$. In addition, the ligand may chemically interact with the solvent, adding further charge. For example, a methoxy-terminated (monofunctional) PEG ligand remains effectively neutral in an aqueous solvent, but charged ligands produce "polyelectrolyte" particles, altering the NP mobility in an even more complex manner than addressed here.[17,35,39,42] For PEGylated Au NPs, which have an uncharged PEG corona, the decrease in electrophoretic mobility that results from a decrease in the total electrophoretic force (due to an increase in the electrophoretic retardation force) and increase of the hydrodynamic drag force can be misinterpreted as a decrease in the Au core surface charge. The following electrokinetic theories for soft composite spheres address important shortcomings of the foregoing classical theories for bare particles.

In transitioning to electrokinetic models for the uncharged ligand-capped NPs depicted in Figure 3, we highlight Ohshima's semianalytical theoretical prediction of the electrophoretic mobility for soft particles with a weakly charged core and an uncharged, permeable corona:[38]

$$\mu = \frac{2}{3}\varepsilon\varepsilon_0\eta^{-1}\zeta_c f_O(\kappa a, b/a, \ell_B/b) \qquad (9)$$

where ζ_c is the core ζ-potential and f_O is a dimensionless function of three dimensionless parameters formed from the core radius a, soft particle radius b, Brinkman screening length ℓ_B[41] (identified by Ohshima as λ),[38] and Debye

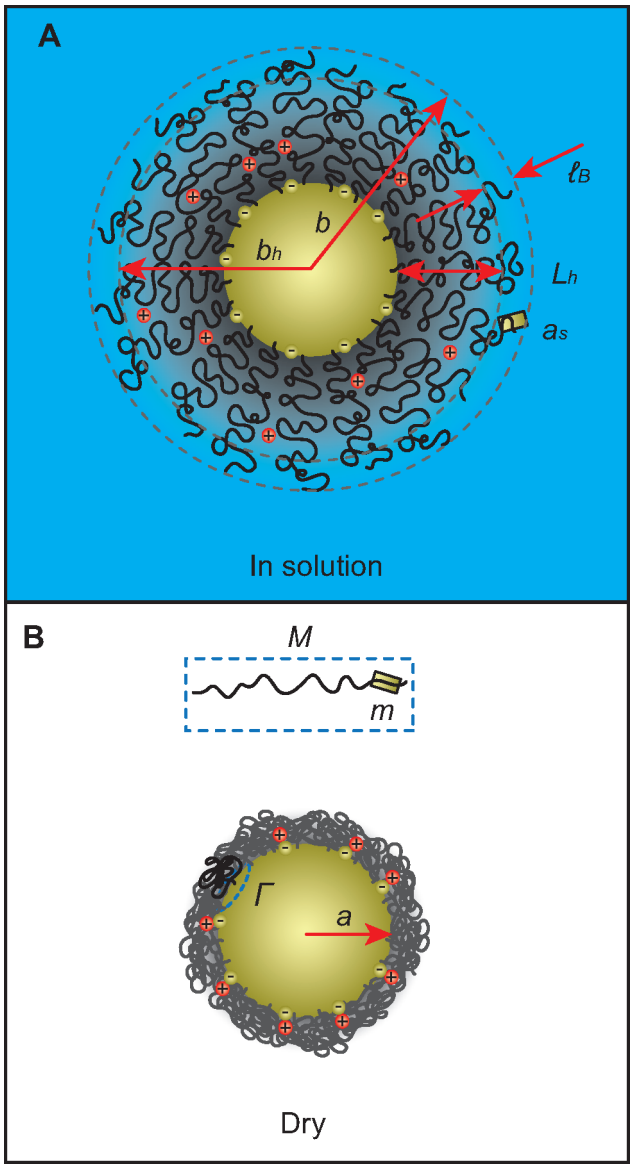

FIGURE 4. Geometrical parameters describing ligand-coated Au NPs, as required to evaluate eq 9 from (A) dispersed (total particle radius b, hydrodynamic radius b_h, hydrodynamic layer thickness L_h, corona Brinkman permeability ℓ_B, and segment hydrodynamic radius a_s) and (B) dry (ligand grafting density Γ, ligand mass M, segment mass m, and core radius a) NP samples, drawing on DLS, TEM, and TGA data.

length κ^{-1} (Figure 4). While a can be readily obtained from transmission electron microscopy (TEM), b is complicated, because the polymer layer, which is not necessarily uniform, has a thickness L that depends on the grafting density Γ and the environment in which it is measured. Note that the NP hydrodynamic radius b_h can be obtained from dynamic light scattering (DLS), furnishing the hydrodynamic layer thickness $L_h = b_h - a$. A reasonable approximation is to let $L_h \approx L - \ell_B$, which enables one to estimate ℓ_B by approximating the porous ligand corona

as a uniform, random configuration of spherical Stokes resistance centers.[41] Accordingly, the ligand segment density n and segment hydrodynamic radius a_s furnish

$$\ell_B^{-2} = 6\pi n a_s F(\phi) \quad (10)$$

where the segment drag coefficient $F \approx 1 + 3(\phi/2)^{1/2} + \ldots$ and the hydrodynamic volume fraction $\phi = n4\pi a_s^3/3 \ll 1$.[41] If the polymer layer is assumed uniform, or has a known (radial) distribution, then n can be obtained from the total ligand volume and knowledge of the monomer segment mass m, total ligand mass M, and grafting density Γ obtained from thermal gravimetric analysis (TGA) (Figure 4). Finally, since b_h depends on ℓ_B, b can be obtained iteratively from knowledge of b_h to obtain n and ℓ_B. The foregoing calculation requires an empirical determination of the segment size a_s, but has the advantage that if this size can be determined for one ligand grafting density and molecular weight, then it is possible to reasonably predict how changing the grafting density and molecular weight will influence electrophoretic mobility.[35] Alternatively, one can simply adopt ℓ_B as an empirical parameter for fixed M and Γ.

Ohshima's eq 9 for electrophoretic mobility is plotted as a function of L/a in Figure 5A for several representative values of κa with $\ell_B/a = 3$. (A Matlab function to evaluate Ohshima's theory with other parameter values is available from the authors.) Here, the Au NP core ζ-potential ζ_c is accounted for by scaling μ with the Au NP core Smoluchowski mobility $\varepsilon\varepsilon_0\eta^{-1}\zeta_c$. Note that Ohshima's theory neglects diffuse-layer polarization and is further limited to uniform polymer layers with low core ζ-potential (practically, $|\zeta_c| \lesssim 2k_BT/e \approx 50$ mV). Numerically exact solutions of the full electrokinetic model, obtained from the MPEK software package are presented in Figure 5B and C for two representative values of $|\zeta_c| > k_BT/e$. (The MPEK software package is available from corresponding author R.J.H.[43]) As expected, these numerically exact solutions correspond exactly with Ohshima's solution when $|\zeta_c| \lesssim k_BT/e$. The ostensible discrepancies at higher Au NP core potentials reflect Ohshima's neglect of diffuse-layer polarization, which becomes significant when the Debye–Hückel approximation breaks down.[39,35] Note that Ohshima's theory tends to overestimate the scaling factor (1 and 2/3, respectively, for the Smoluchowski and Hückel limits), particularly with thin polymer layers

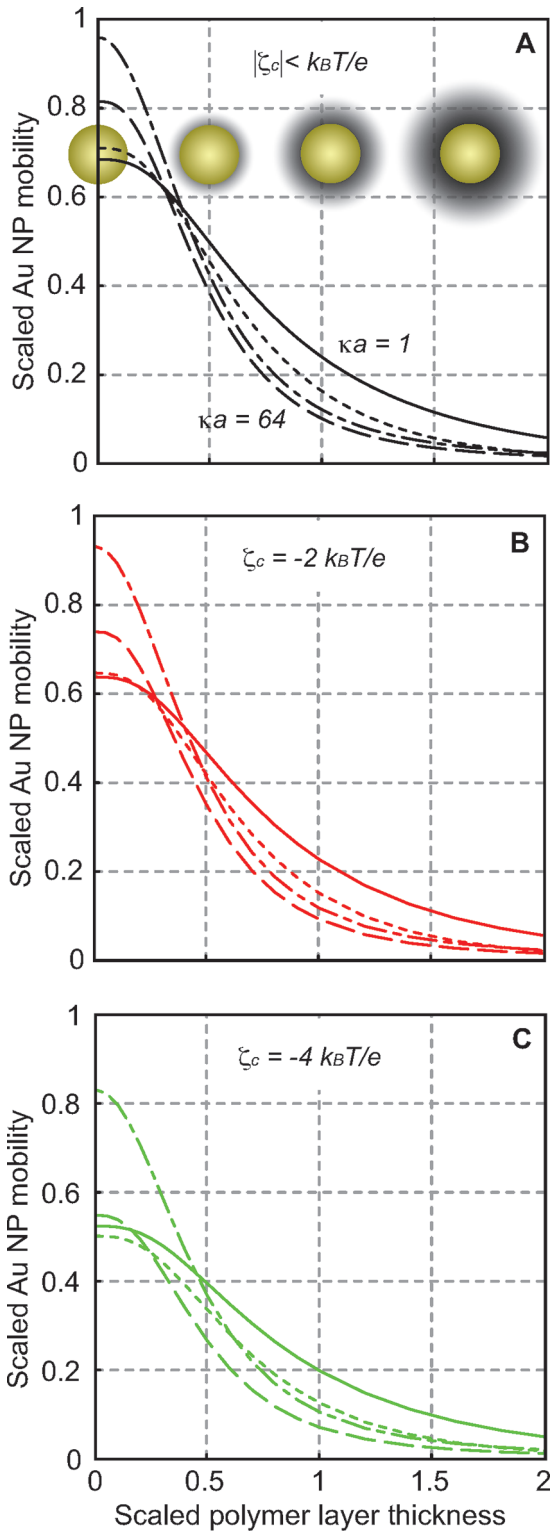

FIGURE 5. PEGylated Au NP electrophoretic mobility μ scaled with the bare Au core Smoluchowski mobility $\varepsilon\varepsilon_0\eta^{-1}\zeta_c$ versus the scaled polymer-layer thickness L/a with $\ell_B = a/3$ and $\kappa a = 1$ (solid lines), 2 (dotted), 8 (dashed), and 64 (dash-dotted). (A) Ohshima's theory[27] for Au NP core ζ-potential $|\zeta_c| \ll k_BT/e$. (B, C) Numerically exact solutions of the soft-sphere electrokinetic model from the MPEK software package[43] with $\zeta_c = -2k_BT/e$ (B) and $-4k_BT/e$ (C).

($L/a \ll 1$) when the diffuse layer is thick ($\kappa L \gg 1$, e.g., low ionic strength) and the core ζ-potential is high ($|\zeta_c| \gg k_BT/e$).

Unfortunately, many NP systems do not satisfy the requirements of Ohshima's theory, because the NP core surface potential $|\zeta_c| > k_BT/e \approx 25$ mV and the polymer layer may not be uniform. Moreover, the complex behavior of end-grafted polymers on highly curved NPs makes it difficult to accurately describe the segment density. Since these complexities must be addressed to successfully apply electrokinetic models, we now turn to the effect of NP surface curvature on grafted polymer conformation.

4. Effect of Nanoparticle Surface Curvature

The ligand thickness is very sensitive to NP surface curvature. Recently, it has been shown that PEG ligand stretching due to surface curvature enhances Au NP decomposition in cyanide environments.[44] Cederquist and Keating recently highlighted the significant role that surface curvature plays on the structure of DNA and oligonucleotides on Au NP surfaces.[45] Stretching can lead to significant deviations from the ideal uniform segment density underlying eq 9, since polymers that are ordered near the NP surface sample more free space at greater distances. Such behavior has been proposed as a means of rationally designing NPs for specific applications, including pH sensitive nanoassemblies.[46]

Dan and Tirrell studied uncharged polymer layers grafted to curved surfaces using self-consistent-field theory (SCFT).[47] These calculations show that the density of chain ends is sensitive to the inner core radius a. Biver et al. used scaling principles embodied in the Daoud and Cotton blob model[48] for spherical micelles to develop a closed-form approximation that captures the effect of surface curvature on the thickness of end-grafted chains at grafting densities where the polymers form chains of blobs at semidilute concentrations.[37] Thus, at moderately high grafting densities, the ligand thickness is easily correlated with the grafting surface curvature, grafting density, and ligand molecular weight, furnishing (at least qualitatively) a hydrodynamic radius $b_h \approx a + L$.

Recently, the present authors[18] investigated 6 nm (diameter) Au NPs with PEG chains ≥1.0 kDa, finding that the hydrodynamic layer thickness L_h (nm) $\approx 6.0[M_{PEG}\ (\text{kDa})]^{0.61}$ with a high grafting density $\Gamma \approx 2.4$ ligands nm^{-2}. The scaling exponent is in good agreement with the 3/5 exponent predicted by Biver et al. when $a \ll L_h$. These considerations furnish a basis for analyzing the effect of NP core size on composite NP radius. Figure 6 shows the predicted ligand thickness for Au NPs with a fixed grafting density (2.4 ligands nm^{-2}) and varying PEG molecular weight for different sized Au NP core radii. From the predicted layer thickness, and knowledge of the ligand molecular weight and grafting density, the polymer segment density can be estimated and, thus, used to predict the layer permeability. It would then be possible to calculate the electrophoretic mobility from numerical solutions of the soft-sphere electrokinetic model.[35] One might even approximate the segment density as being uniform (which it is not when the grafting surface is highly curved) and adopt Ohshima's eq 9 to ascertain the mobility.

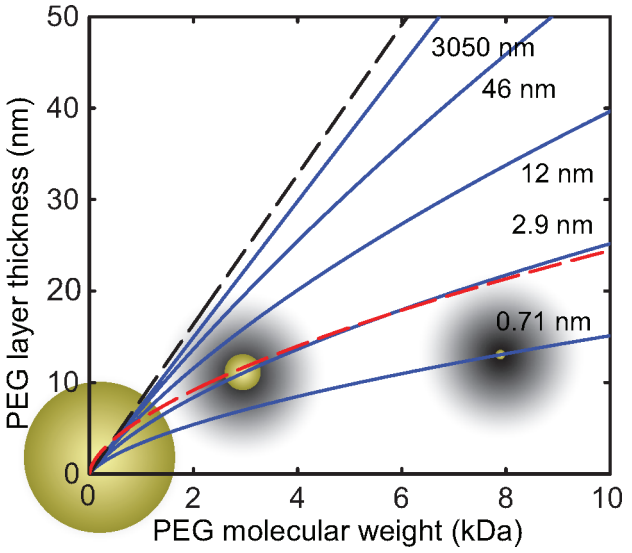

FIGURE 6. PEG layer thickness (solid lines) for PEGylated Au NPs with increasing Au NP core radius a versus PEG molecular weight M_{PEG} according to the semiquantitative scaling model of Biver et al.[37] Also shown are the experimentally determined hydrodynamic layer thickness[18] L_h (nm) $\approx 6.0[M_{PEG}\ (\text{kDa})]^{0.61}$ (red dashed line) and the PEG-chain contour length (black dotted line). Au NPs with decreasing core radii $a \approx$ 12, 2.9, and 0.71 nm (left to right) are placed to identify the PEG molecular weight yielding a fixed composite sphere diameter $2b = 28$ nm.

Several interesting conclusions regarding polymer coated NPs can be drawn from these data. First, recalling that $b = L + a$, one can "tune" the ratio of ligand and solvent occupied volume to that of the core while maintaining a constant overall size. For example, a particle radius $b = 14$ nm with $a \approx 0.71$, 2.9, and 12 nm can be achieved with $M_{PEG} \approx 7.8$, 2.8, and 0.1 kDa, respectively, with the core to soft-volume ratio increasing from 0.01 to 63%. Clearly, the rational design of PEGylated Au NPs and a quantitative prediction of apparent NP ζ-potential and hydrodynamic radius might be achieved if the grafting density can be controlled during NP synthesis. Second, knowledge of the ligand thickness and hydrodynamic radius helps to elucidate the relative contributions of electrostatic and steric forces on PEGylated Au NP dispersions using DLVO theory, which has recently been

undertaken for citrate-capped Au NPs.[49] Considering the interaction between two PEG brushes,[50] one can evaluate the system thermodynamics to rationally predict (and control) NP behavior in environments where electrostatic stabilization fails. In addition, if one were to assume a uniform grafting density for an anisotropic nanomaterial, such as a nanorod (NR), a different polymer layer thickness for "flat" surfaces in comparison to "curved" surfaces would be expected. Indeed, varying these physiochemical properties has recently been proposed by Murphy et al. to be an important direction for future research, including the synthesis of complex nanoarrays.[51] Calculations such as those presented in Figure 6 could direct selective ligand exchange for new self-assembly techniques.

5. ζ-Potential Applications

In addition to using ζ-potentials to qualitatively predict the extent of electrostatic stabilization and specific substrate interactions, the NP surface charge can be inferred from careful consideration of the chemical environment. Such analysis has been demonstrated for citrate-capped Au NPs.[15] Here, we extend ζ-potential measurements for PEGylated Au NPs to provide a quantitative description of the NP surface and highlight applications to drug delivery.[52,53]

We recently reported the Au core ζ-potential of 6 nm (diameter) Au NPs capped with 1, 2, 5, and 10 kDa HS-mPEG.[18] Although the apparent ζ-potentials furnished by ELS mobilities using the Hückel theory were small, a theoretical interpretation of gel electrophoresis data identified a ζ-potential for the "bare" Au core (i.e., the PEGylated Au NPs without a ligand layer) of about −60 mV. These data can be extended to predict the relative composition of the Au NP surface. When $\kappa a \gtrsim 0.5$, the surface charge density is well described by[19]

$$\sigma = \frac{\varepsilon\varepsilon_0 k_B T}{ze}\kappa\left[2\sinh\left(\frac{\zeta ze}{2k_B T}\right) + \frac{4}{\kappa a}\tanh\left(\frac{\zeta ze}{4k_B T}\right)\right] \quad (11)$$

Thus, according to eq 11, ≈33 negative charges reside on the Au NP surface at 40 mM ionic strength ($\kappa^{-1} \approx 1.5$ nm, $\kappa a \approx 2$). These surface charges are likely halides, which are reported to adsorb onto Au[0] (Cl^- ions from Au NP synthesis involving $AuCl^{4-}$ salts and NaCl electrolyte). To further assess this result, we considered Cl^- ions as surface point charges, and PEG-ligands with a "footprint" of ≈0.35 nm^2 from TGA.[56] Thus, assuming a pseudospherical NP radius indicates that ≈84% of the Au surface is occupied by PEG, with ≈3% occupied by Cl^- ions. Given electrostatic and steric interactions, this view of the gold surface seems reasonable. Moreover, from eq 11 with constant surface potential, the surface charge increases linearly with Cl^- ion concentration, in agreement with previous reports for larger bare Au NPs[15] and isotherms reported for Au electrode surfaces.[54] Even at Cl^- ion concentrations of 100 mM, the total area occupied by Cl^{1-} ions due to isothermic adsorption increases to only ≈4.3% of the total Au NP surface.

Interestingly, ≈33 negative charges is consistent with previous reports from this group when loading PEGylated Au NPs with 32 molecules of the photodynamic therapy drug Pc4, with extensive characterization of the conjugates in both cell and mouse studies.[52,53] In this drug−NP conjugate system, the noncovalent drug loading enables efficient delivery, but requires a means of retaining the drug during transport to the cell. From the application of ELS to access the surface charge, it is apparent that the protonated amino moiety of Pc4 would be easily stabilized by an adsorbed halide ion, but not directly bound as for the sulfur analogue.[53] Thus, in addition to hydrophobic forces, which drive the Pc4 molecule into the PEG layer, it seems that the drug molecule can form an ion−contact pair, which stabilizes the molecule during transport. Quantitative analysis of ELS experiments will provide valuable information for future research into the nature of the noncovalent NP−molecule bond, as well as the optimization of drug stability and payload, and, more generally, the design of nanomaterials for biological applications.

6. Conclusion

Electrophoretic light scattering has emerged as a fast and convenient tool for reporting the ζ-potential of capped NPs, but there are subtleties and challenges that must be addressed to correctly interpret the measured electrophoretic mobility. Far-reaching conclusions can be drawn by carefully considering the molecular capping layer. Here, we focused on "bare" particles and uncharged-ligand-capped particles dispersed in symmetrical electrolytes. We reviewed domains in which the Hückel and Smoluchowski approximations are valid, and when Henry's formula and numerical solutions of the standard electrokinetic model should be adopted to interpret ELS data. We explored three complications to the "bare" NP that arise from uncharged polymeric ligands. With NP properties (including core radius, grafting density, and polymer permeability) obtained from complementary TEM, DLS, and TGA data, theoretical predictions of

the core ζ-potential could be achieved with knowledge of the polymer-coated NP electrophoretic mobility. Through this exploration, the promise of rational NP design was reviewed, providing an outlook for ELS in characterizing the surface properties of PEGylated Au NPs (including the provision of relevant evaluation software) with an application to help understand and optimize noncovalent drug–NP conjugates.

R.J.H. gratefully acknowledges support from NSERC and the Canada Research Chairs program.

BIOGRAPHICAL INFORMATION

Tennyson L. Doane obtained his B.S. in chemistry from Eastern Nazarene College, Massachusetts. As an undergraduate, Tennyson interned at Los Alamos National Laboratory in the Earth and Environmental Sciences with Dr. Donald Reed. He is currently a Ph.D. candidate at Case Western Reserve University with a focus on gold nanoparticle transport and spectroscopy.

Chi-Hung Chuang obtained his B.S. and M.S. in chemistry from the National Taiwan University, Taipei. After completing compulsory military service in Taiwan, Chi-Hung was a research assistant at the Institute of Atomic and Molecular Sciences at the Academia Sinica, Taiwan. He is currently a Ph.D. candidate at Case Western Reserve University with a focus on femtosecond spectroscopy of core–shell nanostructures.

Reghan J. Hill obtained his B.E. in chemical and materials engineering from Auckland University, New Zealand, and Ph.D. in Chemical Engineering from Cornell University under Professor Donald L. Koch. Hill was a postdoctoral research associate at Princeton University under Professors Dudley A. Saville and William B. Russel. He is presently an Associate Professor of Chemical Engineering at McGill University where he holds the Canada Research Chair in Colloids for Advanced Materials.

Clemens Burda obtained his Ph.D. from the University of Basel, Switzerland. He was a postdoctoral fellow at the Georgia Institute of Technology with Professor El-Sayed. Currently, he holds faculty positions in Chemistry and Materials Science and Engineering at Case Western Reserve University focusing on nanomaterials chemistry and laser spectroscopy.

FOOTNOTES

*To whom correspondence should be addressed. E-mail: reghan.hill@mcgill.ca (R.J.H.); clemens.burda@case.edu (C.B.).

REFERENCES

1 Corni, I.; Ryan, M. P.; Boccaccini, A. R. Electrophoretic deposition: From traditional ceramics to nanotechnology. *J. Eur. Ceram. Soc.* **2008**, *28*, 1353–1367.

2 Nie, Z.; Petukhova, A.; Kumacheva, E. Properties and emerging applications of self-assembled structures made from inorganic nanoparticles. *Nat. Nanotechnol.* **2010**, *5*, 15–25.

3 Sperling, R. A.; Gil, P. R.; Zhang, F.; Zanella, M.; Parak, W. Biological applications of gold nanoparticles. *Chem. Soc. Rev.* **2008**, *37*, 1896–1908.

4 Tripkovic, D. V.; Strmcnik, D.; van der Vliet, D.; Stamenkovic, V.; Markovic, N. M. The role of anions in surface electrochemistry. *Faraday Discuss.* **2008**, *140*, 25–40.

5 Zukoski, C. F.; Saville, D. A. The interpretation of electrokinetic measurements using a dynamic model of the stern layer: I. The dynamic model. *J. Colloid Interface Sci.* **1986**, *114*, 32–44.

6 Delgado, A. V.; González-Caballero, F.; Hunter, R. J.; Koopal, L. K.; Lyklema, J. Measurement and interpretation of electrokinetic phenomena. *J. Colloid Interface Sci.* **2007**, *309*, 194–224.

7 Smoluchowski, M. V. In Electrische Endosmose und Strö-mungsströme. *Handbuch der Elektrizität und des Magnetismus*; Greatz, L., Ed.; Barth: Leipzig, 1921; Vol. 2; pp 62–366.

8 Bouchard, D.; Ma, X.; Isaacson, C. Colloidal properties of aqueous fullerenes: isoelectric points and aggregation kinetics of C60 and C60 derivatives. *Environ. Sci. Technol.* **2009**, *43*, 6597–6603.

9 Firnkes, M.; Pedone, D.; Knezevic, J.; Döblinger, M.; Rant, U. Electrically facilitated translocations of proteins through silicon nitride nanopores: conjoint and competitive action of diffusion, electrophoresis, and electroosmosis. *Nano Lett.* **2010**, *10*, 2162–2167.

10 Particle Sizing Systems, NICOMP 380 ZLS User Manual (Zeta Potential Theory), 2006.

11 Brookhaven Instruments, Zeta Plus Manual (Theory), 2002.

12 O'Brien, R. W. Electroacoustic effects in a dilute suspension of spherical particles. *J. Fluid Mech.* **1988**, *190*, 71–86.

13 Yariv, E. "Force-free" electrophoresis? *Phys. Fluids* **2006**, *18*, 031702.

14 Daniel, M. C.; Astruc, D. Gold nanoparticles: assembly, supramolecular chemistry, quantumsize-related properties, and applications toward biology, catalysis, and nanotechnology. *Chem. Rev.* **2004**, *104*, 293–346.

15 Agnihotri, S.; Ohshima, H.; Terada, H.; Tomoda, K.; Makino, K. Electrophoretic Mobility of Colloidal Gold Particles in Electrolyte Solutions. *Langmuir* **2009**, *25*, 4804–4807.

16 Perrault, S. D.; Chan, W. C. W. Synthesis and Surface Modification of Highly Monodispersed, Spherical Gold Nanoparticles of 50–200 nm. *J. Am. Chem. Soc.* **2009**, *131*, 17042–17043.

17 Hanauer, M.; Pierrat, S.; Zins, I.; Lotz, A.; Sönnichsen, C. Separation of Nanoparticles by Gel Electrophoresis According to Size and Shape. *Nano Lett.* **2007**, *7*, 2881–2885.

18 Doane, T.; Babar, A.; Cheng, Y.; Hill, R. J.; Burda, C. Electrophoretic Mobilities of PEGylated Gold NPs. *J. Am. Chem. Soc.* **2010**, *132*, 15624–15631.

19 Russel, W. B.; Saville, D. A.; Schowalter, W. R. *Colloidal Dispersions*; Cambridge University Press: New York, 1989.

20 Hunter, R. J. *Foundations of Colloid Science*; Oxford University Press: Oxford, 1987; Vol. 1.

21 Hückel, E. Cataphoresis of Spheres. *Phys. Z.* **1924**, *25*, 204–210.

22 Henry, D. C. Cataphoresis of suspended particles. I. The equation of Cataphoresis. *Proc. R. Soc. London, Ser. A* **1931**, *133*, 106–129.

23 Booth, F. The cataphoresis of spherical, solid non-conducting particles in a symmetrical electrolyte. *Proc. R. Soc. London* **1950**, *203*, 533–551.

24 Overbeek, J. T. G. Theorie der elektrophorese. *Kolloid-Beih.* **1943**, *54*, 287–364.

25 O'Brien, R. W.; White, L. R. Electrophoretic mobility of a spherical colloidal particle. *J. Chem. Soc., Faraday Trans.* **1978**, *74*, 1607–1626.

26 Ohshima, H. A simple expression for Henry's function for the retardation effect in electrophoresis of spherical colloidal particles. *J. Colloid Interface Sci.* **1994**, *168*, 269–271.

27 Ohshima, H. Approximate analytic expression for the electrophoretic mobility of a spherical colloidal particle. *J. Colloid Interface Sci.* **2001**, *239*, 587–590.

28 O'Brien, R. W. The solution of the electrokinetic equations for colloidal particles with thin double layers. *J. Colloid Interface Sci.* **1983**, *92*, 204–216.

29 Burda, C.; Chen, X.; Narayanan, R.; El-Sayed, M. A. Chemistry and Properties of Nanocrystals of Different Shapes. *Chem. Rev.* **2005**, *105*, 1025–1102.

30 Makino, K.; Ohshima, H. Electrophoretic Mobility of a Colloidal Particle with Constant Surface Charge Density. *Langmuir* **2010**, *26*, 18016–18019.

31 Khair, A. S.; Squires, T. M. Ion steric effects on electrophoresis of a colloidal particle. *J. Fluid Mech.* **2009**, *640*, 343–356.

32 Mie, G. Beiträge zur Optik trüber Medien, speziell kolloidaler Metallösungen. *Ann. Phys. (Leipzig, Ger.)* **1908**, *25*, 377–445.

33 Dobrovolskaia, M. A.; Patri, A. K.; Zheng, J.; Clogston, J. D.; Ayub, N.; Aggarwal, P.; Neun, B. W.; Hall, J. B.; McNeil, S. E. Interaction of colloidal gold nanoparticles with human blood: effects on particle size and analysis of plasma protein binding profiles. *Nanomed. Nanotechnol.* **2009**, *5*, 106–117.

34 Niidome, T.; Yamagata, M.; Okamoto, Y.; Akiyama, Y.; Takahashi, H.; Kawano, T.; Katayama, Y.; Niidome, Y. PEG-modified gold nanorods with a stealth character for in vivo applications. *J. Controlled Release* **2006**, *114*, 343–347.

35 Hill, R. J.; Saville, D. A. "Exact" solutions of the full electrokinetic model for soft spherical colloids: Electrophoretic mobility. *Colloids Surf., A* **2005**, *267*, 31–49.

36 de Gennes, P. G. Polymers at an interface; a simplified view. *Adv. Colloid Interface Sci.* **1987**, *27*, 189–209.

37 Biver, C.; Hariharan, R.; Mays, J.; Russel, W. B. Neutral and Charged Polymer Brushes: A Model Unifying Curvature Effects from Micelles to Flat Surfaces. *Macromolecules* **1997**, *30*, 1787–1792.

38 Ohshima, H. Henry function for the electrophoretic mobility of a charged spherical colloidal particle covered with an ion-penetrable uncharged polymer layer. *J. Colloid Interface Sci.* **2002**, *252*, 119–125.

39 Hill, R. J.; Saville, D. A.; Russel, W. B. Polarizability and complex conductivity of dilute suspensions of spherical colloidal particles with uncharged (neutral) coatings. *J. Colloid Interface Sci.* **2003**, *268*, 230–245.

40 Hill, R. J. Hydrodynamics and electrokinetics of spherical liposomes with coatings of terminally anchored poly(ethylene glycol): Numerically exact electrokinetics with self-consistent mean-field polymer. *Phys. Rev. E* **2004**, *70*, 051406.

41 Brinkman, H. C. A calculation of the viscous force exerted by a flowing fluid on a dense swarm of particles. *Appl. Sci. Res. A* **1947**, *1*, 27–34.

42 Rostro-Kohanloo, B. C.; Bickford, L. R.; Payne, C. M.; Day, E. S.; Anderson, L. J. E.; Zhong, M.; Lee, S.; Mayer, K. M.; Zal, T.; Adam, L.; Dinney, C. P. N.; Drezek, R. A.; West, J. L.; Hafner, J. H. Stabilization and Targeting of Surfactant-Synthesized Gold Nanorods. *Nanotechnology* **2009**, *20*, 434005.

43 Hill, R. J. *MPEK-0.02 software package*; McGill University: Montreal, 2010.

44 Mei, B. C.; Oh, E.; Susumu, K.; Farrell, D.; Mountziaris, T. J.; Mattoussi, H. Effects of Ligand Coordination Number and Surface Curvature on the Stability of Gold Nanoparticles in Aqueous Solutions. *Langmuir* **2009**, *25*, 10604–10611.

45 Cederquist, K. B.; Keating, C. D. Curvature Effects in DNA:Au Nanoparticle Conjugates. *ACS Nano* **2009**, *3*, 256–260.

46 Browne, K. P.; Grzybowski, B. A. Controlling the Properties of Self-Assembled Monolayers by Substrate Curvature. *Langmuir* **2010**, *27*, 1246–1250.

47 Dan, N.; Tirrell, M. Polymers tethered to curves interfaces: a self-consistent-field analysis. *Macromolecules* **1992**, *25*, 2890–2895.

48 Daoud, M.; Cotton, J. P. Star shaped polymers: a model for the conformation and its concentration dependence. *J. Phys. (Paris)* **1982**, *43*, 531–538.

49 Kim, T.; Lee, K.; Gong, M. S.; Joo, S. W. Control of Gold Nanoparticle Aggregates by Manipulation of Interparticle Interaction. *Langmuir* **2005**, *21*, 9524–9528.

50 Kim, J. U.; Matsen, M. W. Interaction between Polymer-Grafted Particles. *Macromolecules* **2008**, *41*, 4435–4443.

51 Murphy, C. J.; Thompson, L. B.; Alkilany, A. M.; Sisco, P. N.; Boulos, S. P.; Sivapalan, S. T.; Yang, J. A.; Chernak, D. J.; Huang, J. The Many Faces of Gold Nanorods. *J. Phys. Chem. Lett.* **2010**, *1*, 2867–2875.

52 Cheng, Y.; Samia, A. C.; Meyers, J. D.; Panagopoulos, I.; Fei, B.; Burda, C. Highly Efficient Drug Delivery with Gold Nanoparticle Vectors for in Vivo Photodynamic Therapy of Cancer. *J. Am. Chem. Soc.* **2008**, *130*, 10643–10647.

53 Cheng, Y.; Samia, A. C.; Li, J.; Kenney, M. E.; Resnick, A.; Burda, C. Delivery and efficacy of a cancer drug as a function of the bond to the gold nanoparticle surface. *Langmuir* **2010**, *26*, 2248–2255.

54 Shi, Z. S.; Lipowski, J. Chloride adsorption at the Au(111) electrode surface. *J. Electroanal. Chem.* **1996**, *403*, 225–239.

55 Lei, H. W.; Uchida, H.; Watanabe, M. Electrochemical Quartz Crystal Microbalance Study of Halide Adsorption and Concomitant Change of Surface Excess of Water on Highly Ordered Au(111). *Langmuir* **1997**, *130*, 3523–3528.

56 Wuelfing, W. P.; Gross, S. M.; Miles, D. T.; Murray, R. W. Nanometer Gold Clusters Protected by Surface-Bound Monolayers of Thiolated Poly(ethylene glycol) Polymer Electrolyte. *J. Am. Chem. Soc.* **1998**, *13*, 12696–12697.